Materials & Design 221 (2022) 110938

Contents lists available at ScienceDirect

Materials & Design

journal homepage: www.elsevier.com/locate/matdes

Thermal conductivity of low-density micro-and nanocellular poly (methyl-methacrylate) (PMMA): Experimental and modeling

Ismael Sánchez-Calderón [a,*], Victoria Bernardo [b], Judith Martín-de-León [a], Miguel Ángel Rodríguez-Pérez [a,c]

[a] CellMat Laboratory, Campus Miguel Delibes, Faculty of Science, Condensed Matter Physics Department, University of Valladolid, Paseo de Belén 7, 47011 Valladolid, Spain
[b] CellMat Technologies S.L., Paseo de Belén 9-A, 47011 Valladolid, Spain
[c] BioEcoUVA Research Institute on Bioeconomy, University of Valladolid, 47011 Valladolid, Spain

HIGHLIGHTS

- Measurement and semi-empirical modeling of the thermal conductivity of low-density micro-and nanocellular poly(methyl-methacrylate) (PMMA).
- Production and characterization of poly(methyl-methacrylate) (PMMA) sheets with relative densities ranging 0.08–0.19 and cell sizes between 400–4000 nm.
- Novel method for characterizing the structural factor g from the slope of the thermal conductivity at different temperatures.
- The model allows understanding the influence of each parameter on the total thermal conductivity and provides the minimum values of the thermal conductivities.

GRAPHICAL ABSTRACT

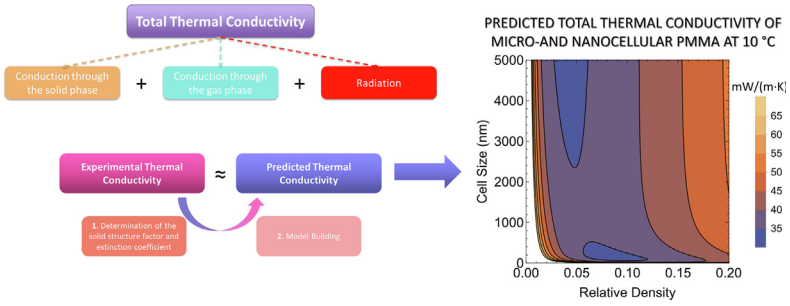

ARTICLE INFO

Article history:
Received 26 February 2022
Revised 8 July 2022
Accepted 8 July 2022
Available online 11 July 2022

Keywords:
Thermal conductivity
Poly(methyl-methacrylate)
Microcellular polymer
Nanocellular polymer
Conduction
Radiation

ABSTRACT

Nowadays, finding new materials with enhanced thermal insulation properties has become a mandatory task to reduce energy consumption and CO_2 emissions. In recent years, nanocellular polymers have aroused great attention due to their very interesting combination of properties, which include reduced conduction through the gas phase thanks to the Knudsen effect.

There are plenty of theoretical works hypothesizing the thermal insulation performance of nanocellular polymers. However, there is a lack of experimental results, especially at low densities. In the present work, the thermal conductivity of low-density microcellular and nanocellular poly(methyl-methacrylate) (PMMA) was measured to evaluate the different heat transfer mechanisms acting on these structures. PMMA foamed sheets with relative densities ranging from 0.09 to 0.18 and cell sizes between 400–4000 nm were produced by gas dissolution foaming using CO_2 as a physical blowing agent. Samples were measured at various temperatures, resulting in thermal conductivities between 37.4 and 46.6 mW/(m·K) at 10 °C. Experimental results have been analyzed to build a semi-empirical model able to predict the thermal conductivity and each heat transfer mechanism contribution. To do this, a novel method to determine the solid structure factor from the slope of the thermal conductivity versus the temperature curve is introduced.

* Corresponding author.
E-mail address: ismaelsc@fmc.uva.es (I. Sánchez-Calderón).

https://doi.org/10.1016/j.matdes.2022.110938
0264-1275/

1. Introduction

The global population is expected to increase by 2.5 billion people by 2050. As economic development and living standards are improving worldwide energy use is expected to rise greatly, especially in the building sector. With no improvements in energy efficiency, the energy demand for buildings is expected to grow by 50% by 2050 [1]. Thus, the building sector is crucial to accomplishing a resource-efficient and low-carbon economy [2]. Since nowadays buildings are responsible for around 40% of the global energy consumption and 36% of the emitted greenhouse gases [3], governments, like the European Union, had established legislative frameworks [4,5] to boost their energy performance. Particularly, more than 40% of the energy used in buildings is destined for climatization, making the thermal insulation performance of buildings a key factor to reduce energy consumption and the CO_2 emissions associated with energy production [2,6].

1.1. Research progress of thermal conductivity of foam materials

The physical parameter used to quantify the thermal insulation performance of a given material is thermal conductivity. It is an intensive physical property that describes heat transport through a body due to a temperature gradient. Currently, the materials used in the building sector (such as polyurethane (PU), mineral wool, expanded polystyrene (EPS), and extruded polystyrene foam (XPS)) are characterized by aged thermal conductivities around 25–40 mW/(m·K) [7]. To further enhance the thermal insulation and meet the new legislation [4,5] there are two possible routes. On the one hand, the solution pass by increasing the thickness of the insulation layer using conventional insulation materials. However, this approach requires acquiring larger amounts of material, with implications for the environment and CO_2 emissions, and implies the reduction of the useful area in buildings. On the other hand, a promising approach goes through developing new thermal insulators with lower thermal conductivity. This alternative would allow not only save energy but also extend the useful area in buildings by obtaining the same insulation with reduced thickness. Therefore, finding new enhanced thermal insulators becomes a mandatory task to improve the building sector's energy efficiency.

In recent years, nanocellular polymers (cell sizes below 1 μm) have aroused great attention due to their very interesting combination of properties: lightweight, low cost, recyclability, reduced thermal conduction through the gas phase, enhanced mechanical properties, etc [8–12]. Particularly, it was claimed several times that these materials could be potentially used as advanced thermal insulators when combining low-densities and nanometric cell sizes, but no experimental data supported these claims [13–15]. The production of nanocellular polymers is still a challenge [16], especially in the range of low density. Furthermore, since fabrication processes are mainly limited to the lab scale, the production of samples with dimensions large enough for characterization is also a complex task [17]. For these reasons, many authors have tried to theoretically predict the thermal properties of these materials [15,18–21]. For instance, Forest et al. proposed an analytical model derived from aerogel studies [15]. This model predicted thermal conductivities as low as 12 mW/(m·K) for nanocellular materials with relative densities between 0.1–0.2 and cell sizes around 100 nm at 27 °C (300 K) [15]. Wang et al. [19] mathematically modeled the thermal transport through a nanocellular polymer. Their model proposed that the contribution of the radiation term starts to be quite significant in nanocellular polymers with low densities. They predicted that the minimum conductivity that can be reached with these materials is not as low as expected. Later, Bernardo and coworkers [20] proved that the transmittance of infrared radiation significantly increases when the cell size is reduced to the nanometric range. As a consequence, low-density nanocellular polymers combine low conduction through the gas phase with a high radiation contribution, leading to a compromise between cell size and density to obtain the best results. However, the transmittance measurements were performed with samples with larger densities than those that should be used for thermal insulation (relative density 0.4). Buahom et al. [21] also developed a mathematical model to predict the thermal conductivity of microcellular and nanocellular polymer foams. They predicted the thermal conductivity of PS and PMMA foams with different relative densities and cell sizes. Particularly, they predicted a minimum of 37 mW/(m·K) for nanocellular PMMA with 0.1 of relative density and 100 nm of cell size at 27 °C (300 K) [21]. The two previous models of the thermal conductivity of PMMA [19,21] were validated using medium and high-density samples, and provided useful insights into the mechanisms acting during heat transfer in these materials. In this work, we prepare a collection of low-density nanocellular materials (cell sizes ranging from 400 nm to 4000 nm and relative densities between 0.09–0.18) and we characterize their thermal conductivity using a heat flow meter. The obtained data is used for determining the fitting parameters of a semi-empirical model to predict the thermal conductivity of PMMA foams.

1.2. Theoretical research on thermal conductivity calculation

In a porous material, the total thermal conductivity (λ_t) can be described as a function of conduction through the solid phase (λ_s), conduction through the gas phase (λ_g), thermal radiation (λ_r), and convection within cells (λ_c), as shown in Equation (1) [22].

$$\lambda_t = \lambda_s + \lambda_g + \lambda_r + \lambda_c \quad (1)$$

However, the contribution of convection can be neglected when the cell sizes are lower than 2 mm [23–27].

1.2.1. Conduction through solid

Conduction through the solid phase depends on the relative density (ρ_r) (defined as $\rho_r = \rho / \rho_s$, where ρ is the density of the porous material and ρ_s is the density of the solid), on the conductivity of the solid matrix (λ_s) (which also depends on the temperature), and on a structural factor g (Equation (2)) [28]. Regarding the solid structure factor (g), it can vary depending on the solid structure of the material, ranging between 0.3–1 for cellular materials [8,28,29] and taking values as low as 0.003 for aerogels [24,30].

$$\lambda_s = g\lambda'_s\rho_r \quad (2)$$

Differences lay in the solid structure connectivity which determines the phonon diffusion throughout the material [31]: while cellular materials present an interconnected solid structure, aerogels present a backbone structure with multiple contact points, which minimizes conduction through the solid phase. Several works propose that g is related to the longitudinal sound speed of the material [31,32] and also to the mechanical properties [33]. Thus, g is a key parameter to predict solid thermal conductivity, but its experimental determination is quite a challenge. For low-density open cell foams, g is known to be 1/3, whereas closed-cell materials are usually modeled considering 2/3 [28]. For nanoporous systems, there is still no agreement on the value of this parameter. In this research, g will be considered as a variable and calculated based on the experimental data.

1.2.2. Conduction through gas

As shown in Equation (3) conduction through the gas phase depends on the porosity (V_f) (calculated as $V_f = 1 - \rho_r$) and the

thermal conductivity of the gas inside the cells λ_g (which also depends on the temperature) [34].

$$\lambda_g = \lambda'_g V_f = \lambda'_g(1-\rho_r) \tag{3}$$

In nanocellular polymers, the appearance of the Knudsen effect reduces the contribution of the thermal conductivity of the gas phase with respect to the equation for conventional materials (see Equation (4)) [8]. This effect implies that when cell size is comparable to or smaller than the mean free path of the gas molecules they collide more often with the cell walls than among them, reducing the energy transfer [35]. Therefore, the conductivity of the gas inside the cells is reduced. It depends on the conductivity of the free gas (λ_{g0}), the cell size (ϕ), and the mean free path of the gas molecules (l_g) once the Knudsen effect is considered. Furthermore, β is a dimensionless parameter that considers the transfer of energy between the gas molecules and the solid structure (it is a function of the specific heat ratio, the thermal accommodation coefficient, and the Prandtl number [35–38]). β value varies from 1.5 to 2 for argon and nitrogen [35], being 1.64 the value for air [36]. According to the theory, the Knudsen effect starts becoming relevant when the cell size is smaller than 100 times the mean free path, $\phi \leq 100\ l_g$ ($\phi \leq 7$ μm for air) [39].

$$\lambda'_g = \frac{\lambda'_{g0}}{1+\frac{2\beta l_g}{\phi}} \tag{4}$$

Furthermore, the mean free path depends on the temperature (T), the pressure (p), and the molecule diameter (d_m) (3.6 Å for air [40]) as shown in Equation (5) [35], where R is the ideal gas constant and N_A the Avogadro's number.

$$l_g = \frac{RT}{\sqrt{2}\pi d_m^2 N_A p} \tag{5}$$

So, the conduction through the gas phase can be now expressed in terms of the cell size, the characteristics of the gas, and the pressure and temperature, as given in Equation (6). This last equation will be used in this work to predict the conduction through the gas phase.

$$\lambda_g = \lambda'_g(1-\rho_r) = \frac{\lambda'_{g0}(1-\rho_r)}{1+\frac{2\beta}{\phi}\frac{RT}{\sqrt{2}\pi d_m^2 N_A p}} \tag{6}$$

1.2.3. Radiation

Radiation heat transfer within porous materials is a diffusion-like process via scattering and absorption of infrared radiation. The contribution of radiation starts to become relevant when the relative density reaches values under 0.2 [23–27] since at higher relative densities the high solid fraction absorbs a great amount of infrared radiation. The radiative part of the thermal conductivity in porous materials is given by Equation (7) [41], where σ is the Stefan-Boltzmann constant, n is the refractive index (considered equal to 1 for low-density cellular materials, and aerogels [24,42]), and K_e is the extinction coefficient of the porous material. The determination of the extinction coefficient of the porous material is essential to predict radiation.

$$\lambda_r = \frac{16n^2\sigma T^3}{3K_e} \tag{7}$$

For conventional foams, there are plenty of works calculating this parameter, both theoretically (by using, for instance, Glicksman, equations [28,42,43]) and experimentally (by measuring transmittance to infrared radiation [42]). Theoretical models proposed up to now and used successfully for micro and conventional foams are not valid in the nanoscale. In nanocellular polymers, it was proved that when the cell size is 10 times smaller than the light wavelength (visible light wavelength is centered around 500 nm), the material became transparent (i.e., the scattering of visible light is negligible) [11,44]. This effect is due to the change of the scattering mechanism from Mie scattering to Rayleigh scattering when the cell size is reduced [44,45]. In the Rayleigh scattering regime, the fraction of scattered radiation is reduced, and further, there is a strong dependency between the cellular structure dimensions (cell size, walls, and struts), acting as the scattering center, and the wavelength of the electromagnetic wave [46,47]. Therefore, a similar trend is expected for infrared radiation, as long as the ratio between the scattering center and the wavelength of the electromagnetic wave (thermal infrared) is in the same range. The thermal infrared radiation at room temperature is centered in a wavelength of 10 μm, then one could expect a modification of the scattering regime for cell sizes under 1 μm. In aerogels, such behavior has been reported. For instance, Heinemann et al. [48] did not observe differences between aerogels with different densities and the bulk material extinction coefficient, meaning that the scattering through the pores (characteristic pore size = 180 nm) is null. Hrubesh et al. [24] claimed that the radiation contribution in aerogels was only associated with the absorption of the solid material, assuming that there is no scattering due to the reduced pore size. For nanocellular polymers, recently, Bernardo et al. [20] determined experimentally the scattering extinction coefficient for nanocellular PMMA for the first time by measuring the transmittance in the infrared region of microcellular and nanocellular PMMA (cell sizes from 14 nm to 20 μm) with constant density. A change in the relation between the extinction coefficient and the cell size was observed for cell sizes around 1 μm (1/10 of the infrared wavelength at room temperature, centered at 10 μm, as said before). Therefore, they concluded that the scattering due to the cellular structure must be considered for larger cell sizes but it can be neglected for very small cell sizes (smaller than 200 nm). This is because the scatter mechanism changes from Mie to Rayleigh when reducing the cell size, meaning that there is a stronger dependency with the wavelength in the scattering process and that the fraction of scattered radiation is sharply reduced. However, the density of the samples considered in that work was high, so the absorption contribution could not be measured. In this work, a method to easily determine the total extinction coefficient of nanocellular polymers (including both the absorption and scattering mechanisms) using thermal conductivity measurements is developed for the first time. The method would be described in detail in Section 4. In essence, the solid structure factor (g) and the extinction coefficient (K_e) are calculated using the experimental thermal conductivity as a function of the temperature. The approach relies on subtracting the solid and gas contributions (both contributions depend on the temperature) to calculate the g factor by iteration with the condition that the thermal conductivity must be 0 mW/(m·K) at 0 K. Once the g factor is calculated, K_e can be easily extract from the slope of the curve λ-T^3 as proposed by Almeida et al. [49]. This method allows calculating K_e in a precise way without using FTIR measurements.

Therefore, in the present work, a new model is developed, combining experimental measurements and semi-empirical equations. The thermal conductivity of low-density microcellular and nanocellular PMMA foamed sheets with relative densities ranging from 0.09 to 0.18 and cell sizes between 400–4000 nm are measured using a heat flow meter (steady-state method) to build the model. As far as the authors know, this is the first time that low-density microcellular and nanocellular PMMA are measured using a heat flow meter (which is the most accurate technique to measure the thermal conductivity of insulating materials [50]). The obtained results allow predicting the contribution of each heat transfer mechanism (conduction through the solid phase, conduction through the gas phase, and radiation) for the nanocellular

samples under study. The trends found in this work can be used to estimate the thermal conductivity of nanocellular PMMA materials with similar characteristics as those measured in this paper (solid thermal conductivity, density, and cell size). Furthermore, the findings of this work would help define the potential and limitations of these novel materials.

2. Experimental

2.1. Materials and sample preparation

PMMA PLEXIGLAS® 7H kindly supplied by Röhm GmbH in the form of pellets was used to produce microcellular and nanocellular polymers by gas dissolution foaming after being thermoformed into sheets of 4 mm thickness. This PMMA is characterized by a melt flow index of 0.77 g/10 min (measured at 230 °C and 2.16 kg) and a glass transition temperature of 110.4 °C measured by DSC (model DSC3+, Mettler).

Fig. 1 shows the experimental procedure to produce the materials used in this work. First, PMMA sheets were cut into samples with dimensions of 50 × 50 × 4 mm^3 to perform the foaming experiments (Fig. 1**a**). Foaming experiments were carried out using a high-pressure vessel (model PARR 4681, provided by Parr Instruments Company). Technical characteristics of the setup can be found elsewhere [51,52]. With this setup, foaming experiments were performed using a two-step gas dissolution foaming process [53]. A collection of foamed samples with different cell size and density were obtained by varying the saturation and foaming conditions. Saturation temperature varied from 25 to 45 °C, saturation pressure varied between 30–31 MPa, foaming time varied from 1 to 5 min, and the foaming temperature was 90 °C. For each foaming condition at least 18 samples were produced using the same nominal processing parameters. The thickness of the foamed samples varies between 8–10 mm depending on the expansion.

From the foamed samples (Fig. 1**b**), samples with dimensions of 50 × 50 mm^2 were cut (Fig. 1**c**). Then, the solid skin was removed using a polisher (LaboPOl2-LaboForce3 (Struers)) to obtain a homogeneous sample to perform an accurate study of the influence of the density and cell size on thermal conductivity. The thickness of the final samples after polishing (Fig. 1**d**) was 7 mm.

Finally, the polished samples were stacked forming a stack of samples (Fig. 1**e**) of at least 150 × 150 mm^2 with a thickness of 14 mm for the thermal conductivity measurements.

2.2. Characterization

2.2.1. Cellular structure

The cellular structure was analyzed using a Scanning Electron Microscope (FlexSEM 1000 VP-SEM). Samples were cooled in liquid nitrogen and fractured to maintain the cellular structure for the microscopic visualization. They were also coated with gold using a sputter coater (model SCD 005, Balzers Union). Several parameters were measured to obtain a complete analysis of the cellular structure. A tool based on ImageJ/FIJI [54] was used to obtain the average cell size in 3D (ϕ_{3D}), the cell size distribution, and the standard deviation coefficient (SD) were obtained (a correction factor of 1.273 [54] was applied to the 2D values measured in the SEM micrograph to obtain the 3D values). The normalized standard deviation coefficient (SD/ϕ_{3D}) was calculated as an indicator of the homogeneity of the cellular structure. In every sample, more than 60 cells were analyzed (i.e., more than 1000 cells per reference material). Cell density (N_v) was determined using Kumar's theoretical approximation [55] (Equation (8)), where A is the analyzed area and n is the number of cells in that area. Finally, cell nucleation density (N_0) was determined (Equation (9)).

$$N_v = \left(\frac{n}{A}\right)^{\frac{3}{2}} \tag{8}$$

$$N_0 = \frac{N_v}{\rho_r} \tag{9}$$

2.2.2. Density

The density of the polished cellular materials was obtained using the water-displacement method based on Archimedes' principle. A density determination kit for an AT261 Mettler-Toledo balance was used. The relative (ρ_r) density was obtained by dividing the foam density between the solid PMMA density ($\rho_r = \rho / \rho_s$, where ρ is the foam density and ρ_s is the density of the solid).

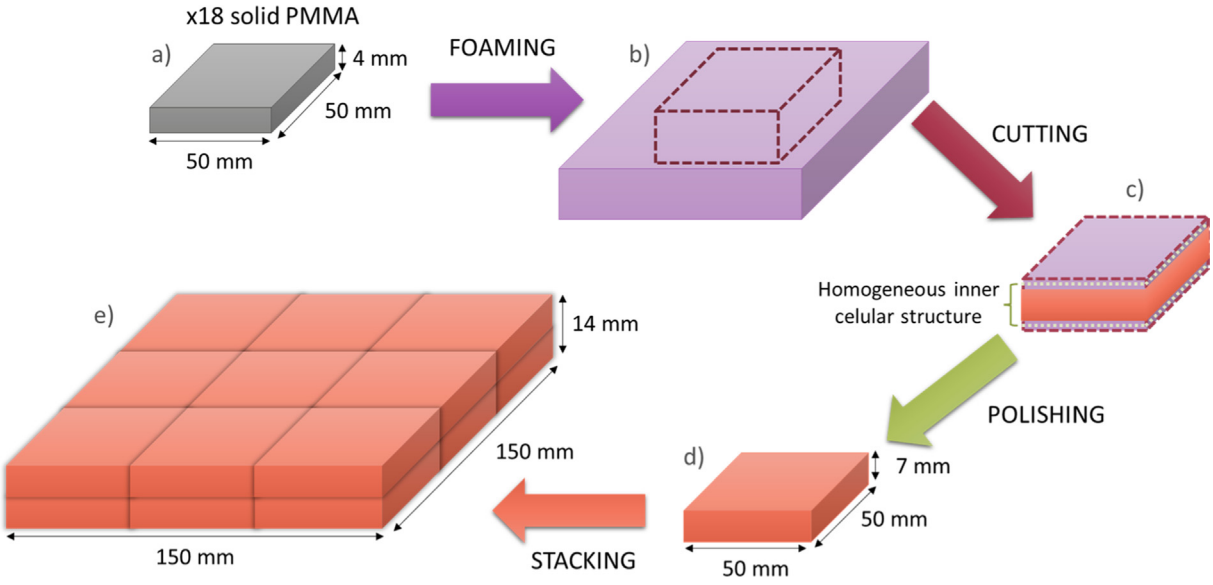

Fig. 1. Experimental procedure to produce the materials used in this work: (a) solid sample, (b) foamed sample, (c) foamed sample after cutting, (d) foam sample after polishing, and (e) stacking of polished foamed samples.

2.2.3. Open cell content

Open cell content (OC) of the polished cellular materials was obtained through Equation (10), using a gas pycnometer (model AccuPyc II 1340, Micromeritics). The gas used was N_2.

$$OC(\%) = \frac{V - V_{pyc}}{V(1-\rho_r)} \cdot 100 \quad (10)$$

Where V_{ext} is the geometric volume and V_{pyc} is the volume obtained from the pycnometric measurement.

2.2.4. Thermal conductivity measurements

Thermal conductivity measurements were carried out using a thermal heat flow meter model FOX 200 (TA Instruments / Laser-Comp, Inc.), which measures according to ASTM C518 and ISO 8301 [56,57]. So, measurements were performed in steady-state conditions. Samples of at least 150 × 150 mm^2 with a thickness of 14 mm were used. For the measurements, the sample was placed between the two plates, promoting a temperature gradient through the material thickness. Measurements were performed at 10, 20, 30, and 40 °C. The temperature gradient (ΔT) was set to 20 °C in every case (i.e., for the measurement at 10 °C, the temperature goes from 0 °C in the upper isothermal plate to 20 °C in the lower one). The active area of the FOX 200 heat flux transducers is 75 × 75 mm^2, so the samples have larger lateral dimensions than the heat flux transducers. The absolute thermal conductivity accuracy for this device is 2%. To fill the remaining volume of the sample holder (with a size of 200 × 200 × 14 mm^3) a polyurethane foam mask was used to avoid air convection. This mask does not affect the measured thermal conductivity since it is not in contact with the heat flux transducers but helps to obtain the correct thermal conductivity of the material. Before this work, several preliminary tests were carried out measuring a conventional thermal insulator of known conductivity using different masks. Results showed that the thermal conductivity of the mask did not affect the accuracy of the measurement. However, without using a mask, the thermal conductivity slightly increased due to convection in the remaining volume. Then, a mask was always used in this work to prevent air convection.

Besides, solid PMMA thermal conductivity was measured as well under the same conditions.

3. Results and discussion

3.1. Sample characterization

Table 1 summarizes the density, relative density, cell size, normalized standard deviation coefficient of the cell size distribution, cell nucleation density, and open cell content of the produced samples. The samples are numbered as a function of their density which ranges between 105 and 218 kg/m^3. The cell size of the samples varies between 394 and 3751 nm. **Figure S1** (Supplementary Information) shows details of the cellular structure of the materials. The normalized standard deviation coefficient takes values lower than 0.7. See **Figure S2** (Supplementary Information) for details about the cell size distributions The normalized standard deviation coefficient takes values lower than 0.7. See **Figure S2** (Supplementary Information) for details about the cell size distributions. In these figures, where it can be observed that the cellular structure is monomodal and cell size distribution is well centered on the mean cell size. The microcellular samples #2, #4, #6, and #8 are more heterogeneous (SD/ϕ_{3D} > 0.5) than the rest of the samples. Samples #5, #7, and #9 are in the nanocellular region with cell sizes below 500 nm, whereas sample #3 is in the upper limit of the nanocellular range (1000 nm). Finally, it is observed that the open cell content increases when the cell size is reduced to the nanoscale. Also, within the nanocellular samples, the open cell content increase as density is reduced. Sample 5 presents the highest open cell content (99.6%). Note that despite the high open cell content of some samples, the cellular structure of all the materials is characterized by showing cell walls and struts. Then the open cell content is due to small holes in the cell walls and not to an absence of walls. This is important because the heat transfer mechanisms might differ for open cell foams without cell walls [21,23]. For instance, in those foams, the absence of cell walls to scatter and absorb radiation lead to higher radiation contribution. In this work, all the samples present similar cellular structures with walls and struts, then the presence of very small holes on the cell walls should not affect the thermal conductivity.

3.2. Thermal conductivity measurements

3.2.1. Microcellular and nanocellular PMMA

Fig. 2**a** shows the experimental thermal conductivity at different temperatures of the samples produced in this work. As observed in Fig. 2**b**, the samples produced in this work fill a wide region in the low-density range (covering relative densities from 0.09 to 0.18) with different cell sizes in the microcellular and nanocellular range. The sample with the lowest density (#1) present the lowest thermal conductivity at 10 °C (37.44 mW/(m·K)). As the measurement temperature increases the thermal conductivity increases. In general, the thermal conductivity increases as density increases. However, some samples (#3, #7, and #9) do not follow this trend, probably due to their smaller cell size which enhances the Knudsen effect, leading to a reduction of the gas thermal conductivity. Note that the reduction of the cell size to the nanoscale also affects the radiation, which is going to be higher than for microcellular foams. Still, the gas thermal conductivity reduction seems to dominate over the radiation rise, decreasing the total thermal conductivity for foams with the same density. For instance, samples #2 and #3 have almost the same density (113 vs 115 kg/m^3) but the cell size of #3 is 3 times smaller (3000 vs 1000 nm), and the total thermal conductivity is smaller. Between #6 and #7, a similar effect occurs, in this case, the difference in densities is slightly higher (173 vs 186 kg/m^3) but also the

Table 1
Density, relative density, cell size, normalized standard deviation coefficient, cell nucleation density, and open cell content of the samples studied in this work.

Sample	ρ (kg/m^3)	ρ_r	ϕ_{3D} (nm)	SD/ϕ_{3D}	N_0 (nuclei/cm^3)	OC (%)
#1	105 ± 12	0.088 ± 0.010	1459	0.41	5.9×10^{12}	5.5
#2	113 ± 12	0.095 ± 0.010	3215	0.70	4.6×10^{11}	10.2
#3	115 ± 9	0.097 ± 0.008	1021	0.45	1.5×10^{13}	38.0
#4	117 ± 17	0.098 ± 0.014	2916	0.59	6.8×10^{11}	2.6
#5	154 ± 10	0.129 ± 0.008	468	0.47	1.0×10^{14}	99.6
#6	173 ± 10	0.146 ± 0.008	2379	0.65	7.1×10^{11}	4.4
#7	186 ± 9	0.155 ± 0.007	408	0.47	1.3×10^{14}	86.1
#8	198 ± 9	0.166 ± 0.008	3751	0.67	1.4×10^{11}	1.6
#9	218 ± 10	0.183 ± 0.009	394	0.43	1.2×10^{14}	73.6

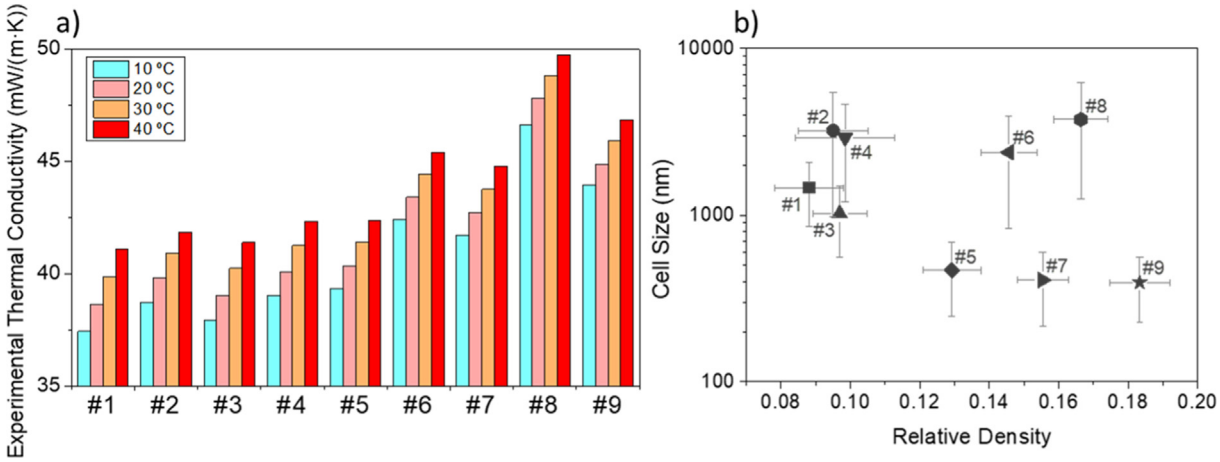

Fig. 2. (a) Experimental thermal conductivity measured at different temperatures of the samples produced in this work. (b) Relative density - Cell size map of the samples produced in this work (the error bar of the cell size corresponds to the cell size distribution standard deviation).

reduction of the cell size (2400 vs 400 nm). Once again, the material with a lower cell size shows a lower thermal conductivity.

As the contribution of the gas thermal conductivity is well known as stated in the theoretical background (Equation (6)), the conductions from conduction through the gas and the sum of conduction through the solid and radiation at 10 °C are presented in Fig. 3**a**. The air thermal conductivity dependence with the temperature in the range between −10 and 60 °C has been considered using Equation (11) (with T in Kelvin) [58].

$$\lambda'_{g0_{-air}}(mW/(m\cdot K)) = 0.07411T + 3.40294 \quad (11)$$

By subtracting the gas thermal conductivity calculated with Equations (6) and (11) to the experimental thermal conductivity (λ_{exp}), the solid phase + radiation contribution to the thermal conductivity can be obtained ($\lambda_s + \lambda_r = \lambda_{exp} - \lambda_g$). On the one hand, it is observed in Fig. 3**a** that in the nanocellular samples #3, #5, #7, and #9 the gas thermal conductivity contribution is reduced in comparison with the microcellular samples with similar density. As a counterpart, it is important to remark that in those samples the contribution of the solid phase + radiation increases with respect to the samples with larger cell sizes. This fact could be related to the increase of the radiation term in nanocellular polymers (recall that for cell sizes below 1 μm the scattering through the cells decrease, increasing the radiation contribution).

As material #5 presents an almost 100% open cell structure (Table 1), it is possible to measure its thermal conductivity as a function of the internal pressure. This measurement will allow confirming the accuracy of Equation (6) to predict the conductivity of the gas phase. For these vacuum measurements, a set-up consisting of a vacuum pump, a vacuum controller, a vacuum valve, and a vacuum bag has been used. Fig. 3**b** shows the thermal conductivity of material #5 at 10 °C at different pressures and the predicted thermal conductivity at vacuum (calculated by adding the gas thermal conductivity as a function of the pressure (Equation (6)) to the solid + radiation term calculated previously from the experimental value). It is observed that the experimental data adjust very well to the vacuum prediction for this material. For the predictions, the average density and cell size are used. Note that there are some uncertainties about the density and the cell size (Table 1), which may cause a slight deviation of the experimental results from the Knudsen prediction (Equation (6)). Anyway, for the maximum vacuum achieved (0.044 mbar) thermal conductivity of 25.74 mW/(m·K) is obtained, really close to the predicted value of 24.90 mW/(m·K) (deviation of 3%). Therefore, we have also confirmed that the gas thermal conductivity can be accurately predicted by using the Knudsen equation (Equation (6)).

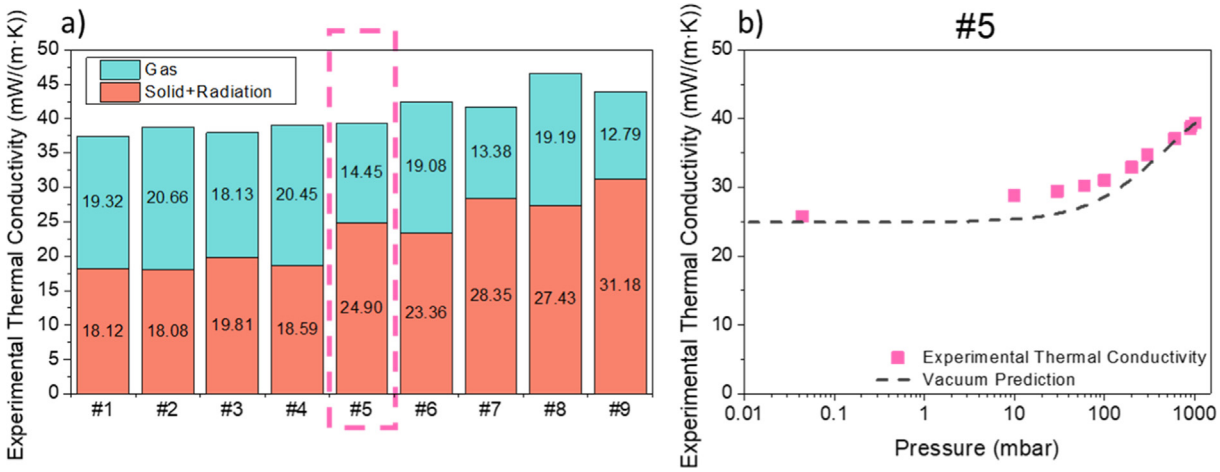

Fig. 3. (a) Gas-phase and solid-phase + radiation contributions to the thermal conductivity at 10 °C. (b) Experimental thermal conductivity of #5 at 10 °C and different pressures and prediction of the thermal conductivity as a function of pressure.

3.2.2. Solid PMMA

Regarding the solid PMMA thermal conductivity, results are shown in Fig. 4. It is observed that as the temperature increases the thermal conductivity of the PMMA increases from 174.0 mW/(m·K) at 10 °C to 180.1 mW/(m·K) at 40 °C. This temperature dependency must be taken into account in the following calculations. Therefore, the solid thermal conductivity of the PMMA (λ_{s_PMMA}) as a function of the temperature (in Kelvin) can be obtained by linear fitting (Equation (12)).

$$\lambda'_{s\_PMMA}(mW/(m\cdot K)) = 0.2060T + 115.5811 \quad (12)$$

4. Model: Experimental determination of the solid structural factor and the extinction coefficient

The total thermal conductivity (in mW/(m·K)) is stated by Equation (13) (obtained after substituting Equations 2, 6, 7, 11, and 12 in Equation (1)). Recall that this equation takes into account the dependence of the thermal conductivity of the solid PMMA with temperature measured experimentally. If this model is applied to other PMMA grades with a different thermal conductivity versus the temperature curve, the solid contribution should be adjusted. The only unknown parameters in this equation are the solid structural factor, g, and the extinction coefficient, K_e. As commented in the introduction, there is a lack of information regarding these two parameters for nanocellular polymers. With the experimental results obtained for the different samples and the dependence of the conductivity with the temperature, it is possible to calculate these two parameters to create a semi-empirical model that would allow calculating these parameters based on the characteristics of the sample (density and cell size).

The strategy followed is summarized in Fig. 5. Meanwhile, Fig. 6 shows an example of the method applied to material #5. First of all, it is necessary to subtract the solid and gas contribution from the experimental thermal conductivity (Fig. 6**a**). As the radiation depends on T^3, the experimental extinction coefficient can be extracted from the fitting slope, as proposed by Almeida et al. [49]. However, in our work the solid structure factor is unknown, and it affects the fitting slope and the y-intercept. Then, it is necessary to determine the structural factor first to then calculate the extinction coefficient. Note that this method allows calculating K_e in a precise way without using FTIR measurements.

$$\lambda_t(mW/(m\cdot K)) = (0.2060T + 115.5811)g\rho_r + \frac{(0.07411T + 3.40294)\cdot(1-\rho_r)}{1+\frac{2\beta}{\phi}\frac{RT}{\sqrt{2}\pi d_m^2 N_A p}} + \frac{16n^2\sigma T^3}{3K_e}\cdot 1000 \quad (13)$$

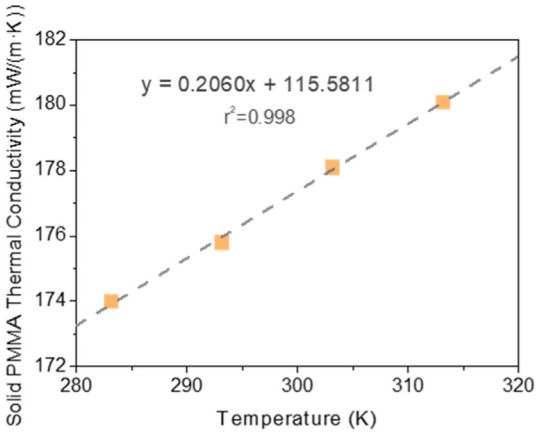

Fig. 4. Solid PMMA thermal conductivity as a function of the temperature.

To calculate g, firstly, a trial solid structure factor, g_{trial}, is used to calculate λ_s at each T (using equations (2) and (12)) and determine a provisional λ_r by subtraction to the experimental value (in Fig. 6**a**, g_{trial} = 0.4 is used as a first approach). Recall that the gas conductivity λ_g is calculated at each temperature using Equations (6) and (11). Then, knowing that the y-intercept must be 0 (because when the temperature is 0 K the radiation is 0 mW/(m·K)), the solid structure factor can be obtained by proving different g_{trial} values. For each g_{trial} the supposed radiation conductivity is calculated as a function of the temperature (Fig. 6**b**). From the linear fit of the proposed solid structure factors (g_{trial}) (Fig. 6**c**) the solid structure factor that leads to y-intercept = 0 can be determined, that is, the accurate experimental g factor, g_{exp}. Finally, using the g_{exp} of each material the real radiation contribution can be calculated. In addition, from the fitting slope of the radiation conductivity vs the temperature cube the experimental extinction coefficient of each material can be obtained (Fig. 6**d**).

Table 2 summarizes the solid structure factor and experimental extinction coefficient for each material calculated as previously commented. Also, the relative extinction coefficient (experimental extinction coefficient divided by the relative density) is included. As the radiation depends on the amount of solid material (i.e., on the density), the relative extinction coefficient allows comparing samples with different densities.

On the one hand, the solid structure factor ranges between 0.85 and 0.95. Up to precision, no relation between the solid structure factor and the cell size or relative density of the samples is observed. The calculated g factor using this methodology is higher than usual predictions for low-density foams [28]. This discrepancy might be related to the assumed thermal conductivity of the solid phase. In this work, we assume that the conductivity of the PMMA in the microcellular and nanocellular polymers is the same as the conductivity of the polymer in a solid sheet. However, this may not be the case: the polymer is stretched in the cell walls, which can result in a higher conductivity than that of a free configuration (like a sheet). Then, the calculated g factors are greatly determined by this assumption. However, for the model, the important parameter is the product between λ_s and g, that is, the effective conductivity through the solid phase in the foam. With the hypothesis of the model, we can accurately predict the contributions of each heat transfer mechanism, as will be explained in the next section.

On the other hand, the experimental extinction coefficient ranges between 14 and 42 cm^{-1}. The extinction coefficient was then calculated using a range of temperatures from 10 to 40 °C. It is observed that as the cell size is reduced, the relative extinction coefficient is reduced (Fig. 7). The trend is potential, meaning that the scattering of infrared radiation decreases drastically when the cell size is reduced. This result matches the experimental results [20] and the theoretical models [19,21] previously reported in the literature. Furthermore, a change in the trend is observed for cell sizes around 1 μm reinforcing the idea of Bernardo et al. [20] that the scattering due to the cellular structure must be considered for larger cell sizes but it can be neglected for very small cell sizes. Finally, a theoretical extinction coefficient that depends on the cell size and the relative density (Equation (14)) is calculated by fitting the relative extinction coefficient as a function of the cell size. Recall that the samples analyzed cover a range of cell sizes between 400–4000 nm and relative densities ranging from 0.09 to 0.18. Then, Equation (14) is accurate within this range and for samples with a similar structure (as previously commented, open cell foams without cell walls might show a different behavior towards radiation). Out of this range, we will use this equation to predict trends, but results must be always considered as estimations, as will be explained later.

$$K_{e\_th} = \left(5.6712\cdot 10^6 \phi^{0.4264}\right)\rho_r \quad (14)$$

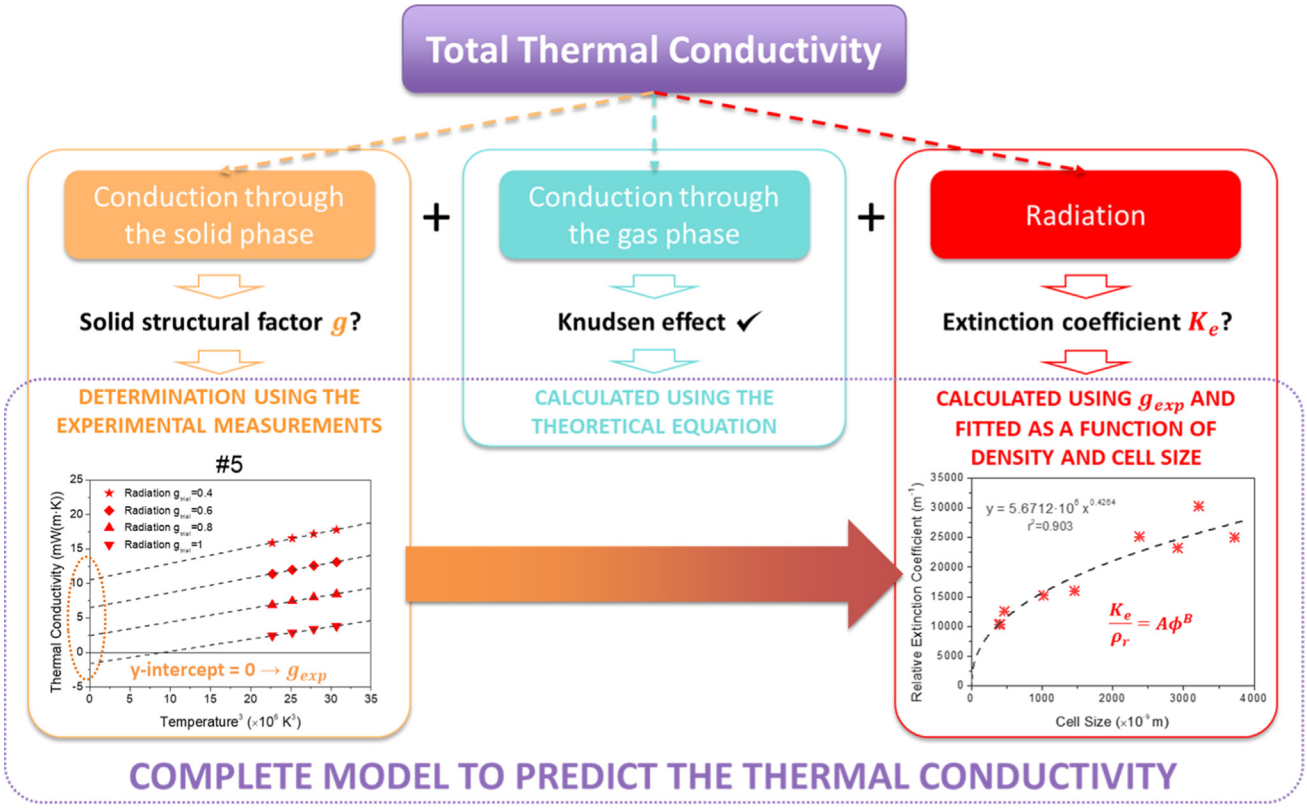

Fig. 5. Strategy to determine the solid structural factor and the experimental extinction to build the model.

The last step to construct a functional model (Fig. 5) is to use the calculated *g* and K_e values to provide a complete equation. Regarding K_e, the theoretical equation (Equation (14)) can be used to obtain its dependency as a function of the density and the cell size. For the structural factor, there are no clear trends, and all the materials present similar g factors with ± 2.4% deviation. Therefore, to build the model, the theoretical solid structure factor is taken as an average of the obtained solid structure factors. An average value of $g = 0.89 \pm 0.03$ has been obtained. Note that, out of the range of densities and cell sizes studied in this work, the *g* factor might be smaller or dependent on the structural characteristics of the foam. Finally, by substituting the value of the theoretical solid structure factor and the theoretical extinction coefficient in Equation (13), the total thermal conductivity as a function of the cell size, the relative density, pressure, and temperature can be obtained (Equation (15)). Note that Equation (15) is strictly accurate for PMMA materials with characteristics within the range under study (relative densities between 0.09–0.18 and cell sizes from 400 to 4000 nm). This equation is used in this work to calculate the contributions of each heat transfer mechanism for the samples analyzed (section 5.1). In addition, we will use Equation (15) to estimate the thermal conductivity as a function of the cell size and density within and out of the range under study (section 5.2). These last predictions must be considered taking into account the possible limitations of the model.

$$\lambda_t(mW/(m\cdot K)) = (0.2060T + 115.5811)0.89\rho_r + \frac{(0.07411T + 3.40294)\cdot(1-\rho_r)}{1+\frac{2\beta}{\phi}\frac{RT}{\sqrt{2}\pi d_m^2 N_A p}} + \frac{16n^2\sigma T^3}{3\left(5.6712\cdot 10^6\phi^{0.4264}\right)\rho_r}\cdot 1000 \quad (15)$$

5. Model: Validation with the experimental results and predictions

5.1. Comparison of the model predictions with the experimental results

Using Equation (15) it is possible to predict the conductivity of the samples measured in this work. First of all, in Fig. 8 a comparison between the experimental and predicted thermal conductivities is presented. On the one hand, it is observed that the accuracy of the model is high (Fig. 8**a**) with, in general, relative errors below 1.5% (Fig. 8**b**). The relative error of #6 is slightly higher (3%) but still low. Furthermore, the accuracy of the predictions seems to not depend on the temperature since the mean error is the same (1.1%) at 10 °C and 40 °C. Although the model is prepared based on the experimental data and it makes sense that similar data are obtained with the predictions, the fact that the values obtained, even at different temperatures, are so close to the real one makes the model gain strength in this range (micro-nanocellular PMMA with relative densities ranging 0.09–0.18, cell sizes between 400–4000 nm and measured at mean temperatures from 10 to 40 °C). This also confirms that the approximations and considerations used are correct.

Fig. 8**c** shows the calculated thermal conductivities of PMMA foams at 10 °C and their contributions from radiation and conduction through the gas and the solid. The model predicts that in the nanocellular materials (#3, #5, #7, and #9) the radiation contribution is much higher than in the microcellular samples with similar or even lower densities. For instance, for samples around 115 kg/m^3, the radiation contribution is 4.5 mW/(m·K) for the nanocellular material (12% of the total thermal conductivity) and 2.8 mW/(m·K) for the microcellular samples (7.3% of the total thermal conductivity).

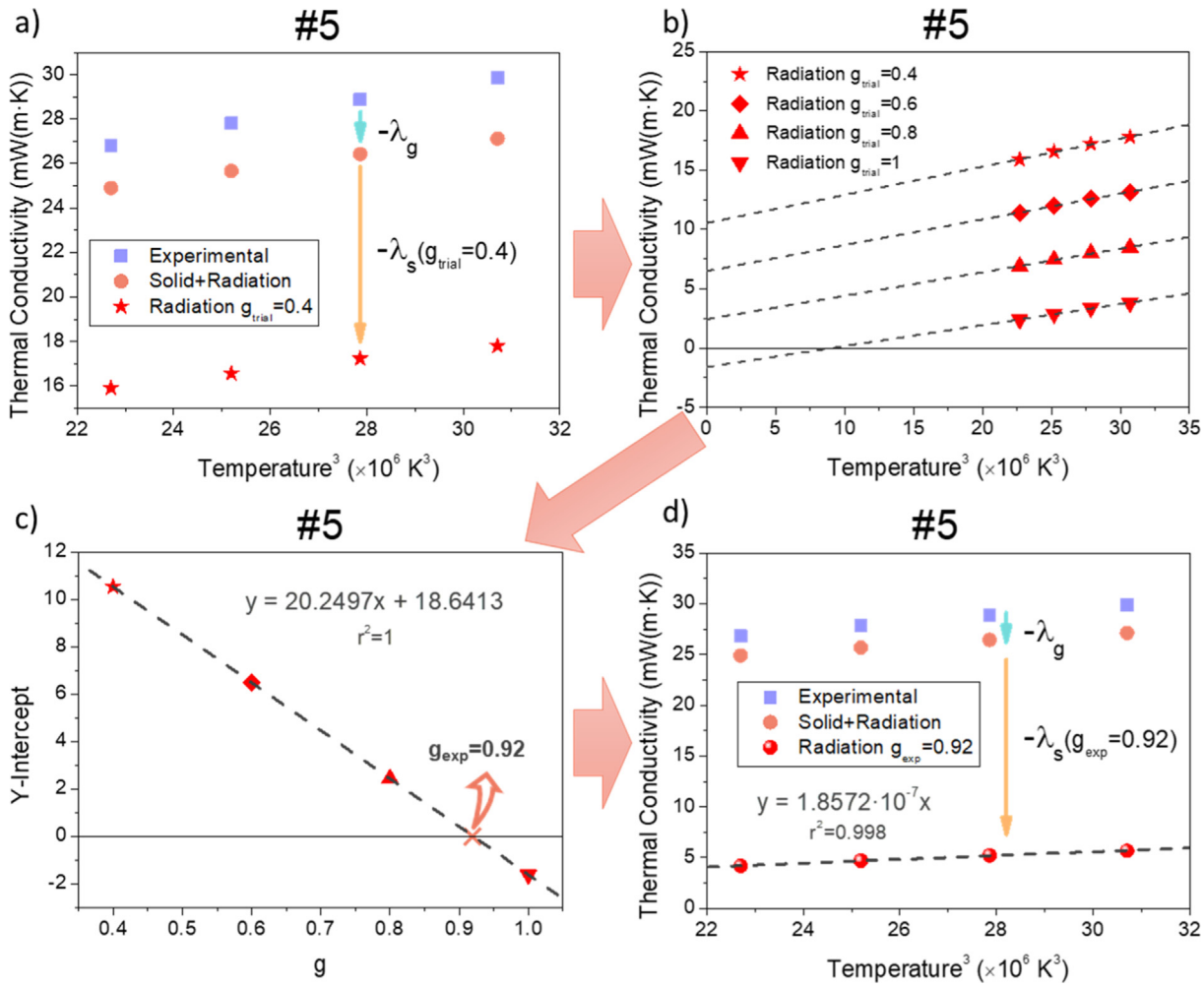

Fig. 6. Example of steps followed to determine the solid structure factor and the experimental extinction coefficient of sample #5: (a) extraction of the gas and solid thermal conductivity from the experimental thermal conductivity at different temperatures using a provisional g_{trial} factor, (b) radiation contributions by using different solid structure factors (g_{trial}), (c) obtention of the proper solid structure factor g_{exp} and (d) obtention of the proper radiation contributions using the g_{exp} and calculation of the extinction coefficient fitting the slope (experimental extinction coefficient).

Table 2
Solid structure factor, experimental extinction coefficient, and relative extinction coefficient of the materials produced in this work.

	Solid	Radiation		
Sample	g_{exp}	K_e (m^{-1})	K_e (cm^{-1})	K_e/ρ_r (m^{-1})
#1	0.87	1416.86	14.17	16057.70
#2	0.95	2876.53	28.77	30292.68
#3	0.90	1474.64	14.75	15259.35
#4	0.91	2287.13	22.87	23262.24
#5	0.92	1628.30	16.28	12582.31
#6	0.85	3658.28	36.58	25163.90
#7	0.89	1615.90	16.16	10394.15
#8	0.89	4163.66	41.64	25024.00
#9	0.87	1899.90	19.00	10371.04

5.2. Effect of the cell size and density on the thermal conductivity

In Fig. 9**a, 9b, and 9c** a map of thermal conductivity as a function of the cell size and the relative density is presented, assuming 10 °C of temperature and ambient pressure. Also, the evolution of the contributions to the total thermal conductivity as a function of the cell size for a fixed density of 100 kg/m^3 is included in Fig. 9**d**. Predictions in the low-density range (relative density below 0.2) are presented for cell sizes below 5 μm. Note that in this map, Equation (15) is used for cell sizes smaller and larger than those of the samples used to create the model. Then, the predictions displayed in Fig. 9 should be considered as estimated trends based on the experimental results found in this paper. It is observed that two minimum regions are predicted, with thermal conductivities around 34 mW/(m·K). The first one appears for cell sizes higher than 3500 nm and relative densities between 0.02 and 0.07 (Fig. 9**b**). The other minimum appears in the nanocellular region for cell sizes around 100–200 nm relative densities between 0.07 and 0.1 (Fig. 9**c**) due to the Knudsen effect. When the cell size of nanocellular foams is reduced, the contribution of the gas phase

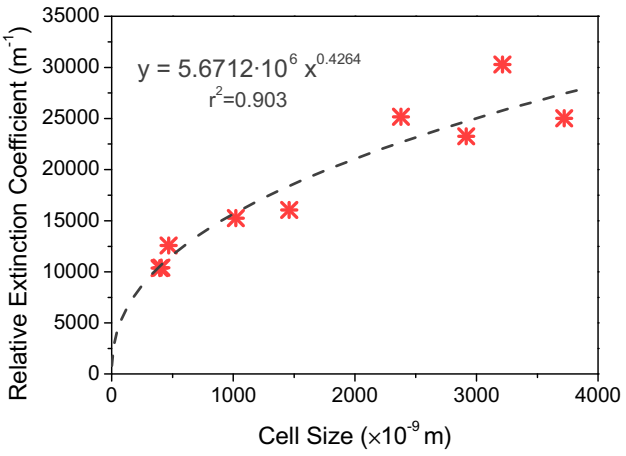

Fig. 7. Relative extinction coefficient as a function of the cell size and exponential fitting. Determination of the theoretical extinction coefficient.

decreases (Fig. 9**d**). Note that in both cases the predictions are beyond the range of densities and cell sizes used to develop the semi-empirical model. However, both minimums can be explained based on theoretical considerations, validating the trends predicted. On the other hand, the theoretical extinction coefficient has been defined as a function of the cell size and relative density. Thereby, the extinction coefficient increases linearly with the relative density and exponentially with the cell size. As the extinction coefficient increases, the contribution of radiation decreases. Both mechanisms, reduction of the gas contribution and increase of the radiation term compete. Therefore, for a given relative density, there is always a minimum of thermal conductivity for a certain cell size as shown in Fig. 9**d**. For relative densities above 0.05, the minimum appears for nanometric cell sizes. However, at lower relative densities the minimum is in the microscale. Both minima are similar, being the value obtained with nanocellular polymers slightly lower. These results agree with the ones for PMMA foams obtained by Buahom et al. [21]. In that work, a minimum was detected for a foam with cells around 100 μm and 40 expansions (relative density of 0.025), out of the scope of our work. Regarding the nanocellular region (cells below 1 μm), Buahom and coworkers found a minimum value of 37 mW/(m·K) for a cell size of 100 nm and a relative density of 0.1. Then, the trend is similar between that theoretical work and our semi-empirical model, despite the differences in the parameters used in both works (Buahom uses a temperature of 300 K and the thermal conductivity of PMMA measured by TPS is 210 mW/mK). In fact, if we apply the semi-empirical model developed in this work for the same nanocellular PMMA (0.1 of relative density and 100 nm of cell size) at the same

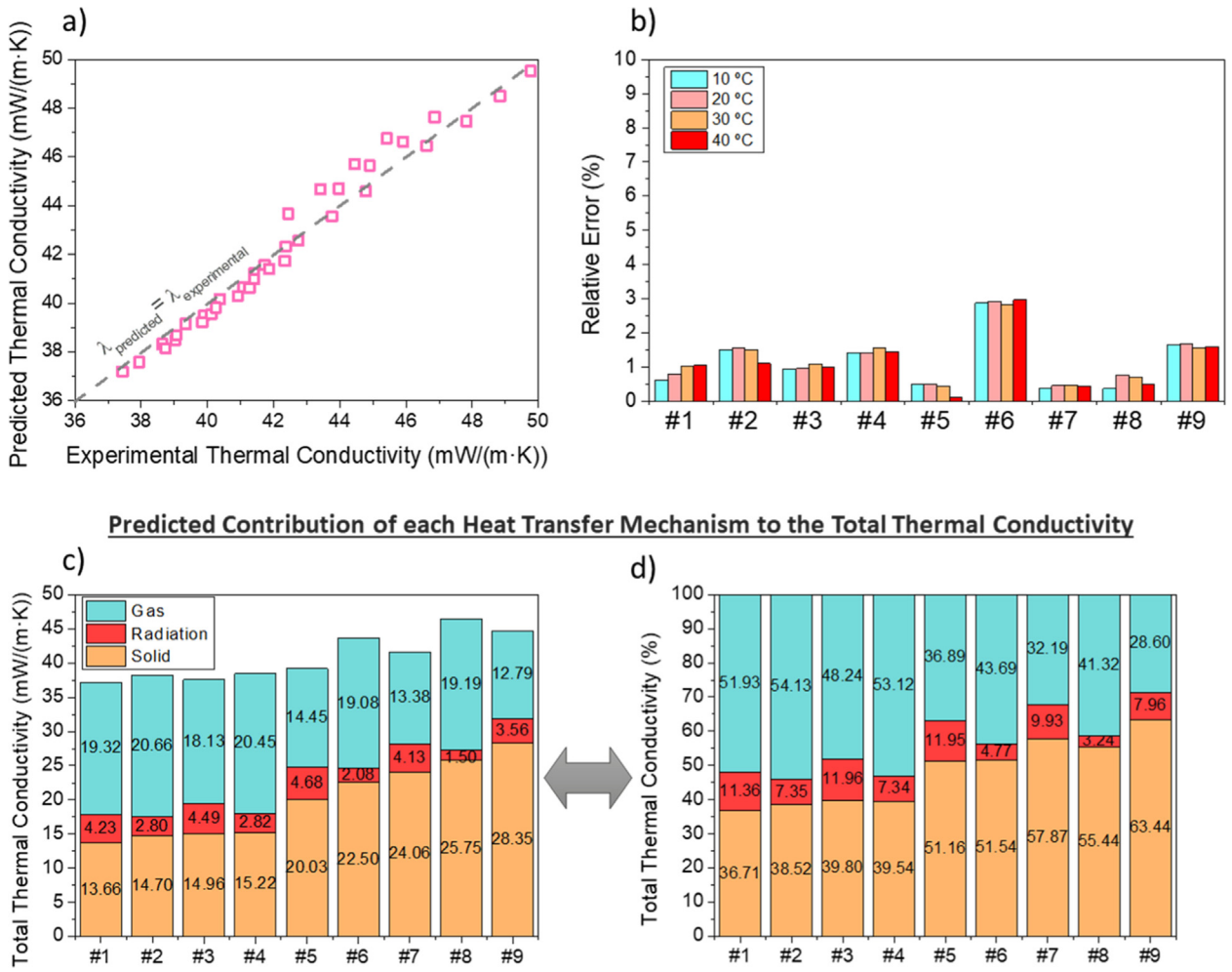

Fig. 8. Comparison between the experimental and predicted thermal conductivities: (a) predicted vs experimental thermal conductivities, (b) relative error on the predictions, (c) predicted contribution of each transfer mechanism to the total thermal conductivity at 10 °C in mW/(m·K), and (d) predicted contribution of each transfer mechanism to the total thermal conductivity at 10 °C in % of the total thermal conductivity.

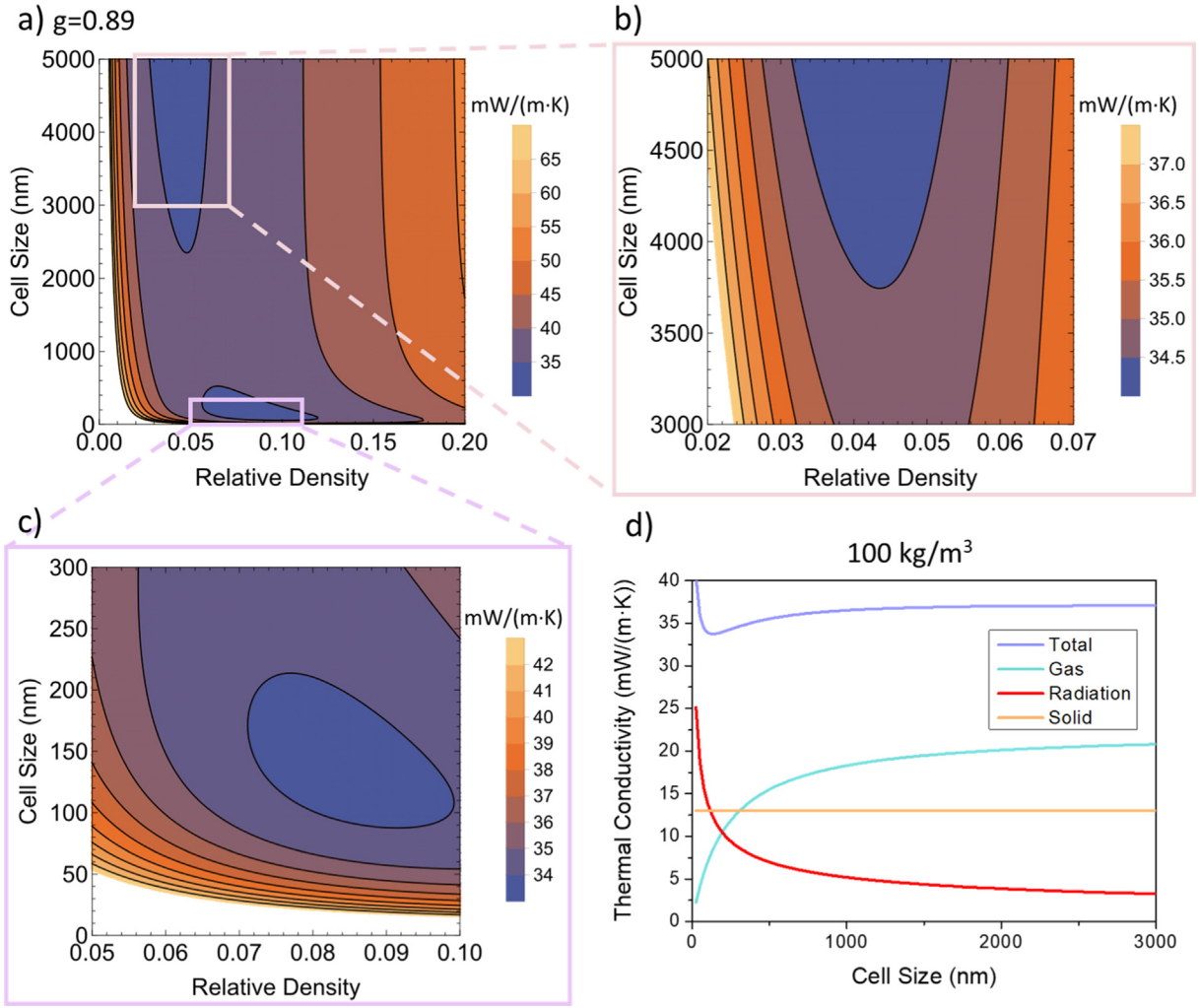

Fig. 9. Predictions based on Equation (15) of thermal conductivity as a function of the cell size and the relative density assuming 10 °C of temperature, ambient pressure and using g = 0.89: (a) full map, (b) zoom of the microcellular minimum region and (c) zoom of the nanocellular minimum region. (d) Evolution of the contributions to the total thermal conductivity as a function of the cell size for a fixed density of 100 kg/m^3.

temperature (300 K), the predicted value is 36.6 mW/(m·K), which is almost the same value reported in [21]. This agreement between both models (theoretical and semi-empirical) reinforces the validity of our model to predict the thermal conductivity of nanocellular PMMA even in a region beyond the range in which the models were tested (Buahom et al. [21] theoretical model) or built (present semi-empirical model).

5.3. Effect of the structural parameter (g) on the thermal conductivity

Finally, note that all the samples produced in this work present similar cellular structures (see **Supplementary Information section S1**) leading to similar structure factors (around 0.9) as seen before. However, it is established that this value can be reduced in nanoscale structures such as aerogels. Therefore, to explore all the possible nanocellular structures, in Fig. 10 a map of thermal conductivity as a function of the cell size and the relative density is presented assuming 10 °C of temperature and ambient pressure as before but using different solid structural factors (g = 0.7, g = 0.5, and g = 0.3). Is important to remark, that these predictions are beyond the range in which the developed semi-empirical model was built. As commented previously, the cellular structure configuration might also affect radiation. Hence, these predictions aim to demonstrate the effect of the structural factor g on thermal conductivity. It is observed that as the structure factor is reduced the minimum of the thermal conductivity decreases (due to the lower contribution of the solid phase) moving to higher relative densities and smaller cell sizes. For instance, for a structure factor of 0.5 (Fig. 10**b**) the thermal conductivity minimum is around 27 mW/(m·K) (0.13 of relative density and 90 nm); whereas for a structure factor of 0.3 (Fig. 10**c**), the minimum is approximately 22 mW/(m·K) (0.18 of relative density and 70 nm).

As previously commented, for low-density foams g factors of 0.3–0.6 are usually reported [28,59,60]. Then, it is plausible to assume that nanocellular polymers with lower densities or different topologies of the cellular structure could lead to really low thermal conductivities, below 27 mW/(m·K) or even 22 mW/(m·K). However, to reach such low values, the configuration of the solid polymer must be different from the structures observed in the samples of this work looking for structures with a larger phonon scattering and lower values of g. As commented in Fig. 10, with the materials produced up to now a minimum of 34 mW/(m·K) is expected. Then, to move a step forward in the field of nanocellular polymers, new structures must be developed. Otherwise, radiation contribution is also high. To further reduce the conductivity, radiation should be blocked to compensate for the reduced scattering and improve the performance of these materials.

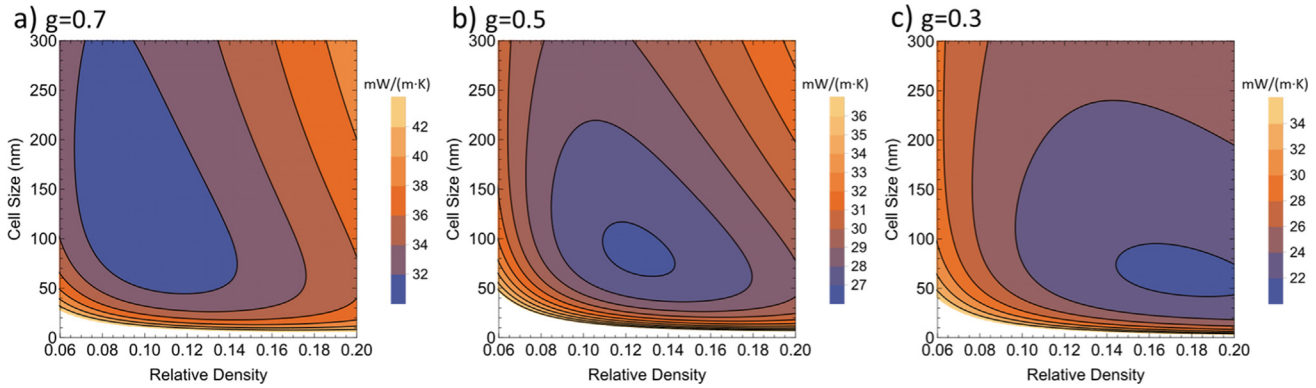

Fig. 10. Map of thermal conductivity as a function of the cell size and the relative density assuming 10 °C of temperature and ambient pressure using different structure factors: (a) g = 0.7, (b) g = 0.5, and (c) g = 0.3.

6. Conclusions

In this work, the thermal conductivity of low-density microcellular and nanocellular PMMA large foamed sheets is measured at different temperatures to develop a semi-empirical model to predict the thermal conductivity based on experimental results. PMMA foamed sheets with relative densities ranging from 0.09 to 0.18 and cell sizes between 400–4000 nm have been produced by gas dissolution foaming using CO_2 as a physical blowing agent. These materials present thermal conductivities between 37.4 and 46.6 mW/(m·K) at 10 °C.

The thermal conductivity results have been deeply analyzed to study the contribution of each heat transfer mechanism (conduction through the solid phase, conduction through the gas phase, and radiation). A novel method to determine the solid structure factor from the slope of the thermal conductivity versus the temperature curve has been introduced. In general, thermal conductivity increases with density. However, when the cell size is reduced below the micron the Knudsen effect plays a key role, leading to a drastic reduction of the gas thermal conductivity, decreasing the overall thermal conductivity. As a counterpart, the reduction of the cell size below the micron implies an increase in the radiation contribution for low-density foams due to reduced cell scattering of the infrared radiation. Therefore, there is a compromise between these two factors (relative density and cell size) to produce an optimum material with minimum thermal conductivity.

Thus, a semi-empirical model able to predict the thermal conductivity of low-density microcellular and nanocellular PMMA is developed. The experimental data are used to calculate the structural factor and the extinction coefficient of nanocellular polymers. The semi-empirical model depends only on the properties of the polymer foam (relative density and cell size) and the measurement conditions (temperature and pressure), and it is valid for PMMA-based materials with relative densities between 0.09–0.18 and cell sizes from 400 to 4000 nm. Predictions for a PMMA-based material (calculated at 10 °C, ambient pressure, and using g = 0.89) show two regions with a minimum of thermal conductivity around 34 mW/(m·K). The first one, situated in the microcellular region, is related to the cell scattering of the radiation (relative densities around 0.04 and cell sizes above 3000 nm) whereas the second one, situated in the nanocellular region, is due to the Knudsen effect (relative densities around 0.08 and cell sizes around 140 nm). However, for different structural factors (g lower than 0.89), the predicted conductivity can be as low as 22–27 mW/(m·K). The model allows understanding the influence of each parameter on the total conductivity, as well as the expected minimum conductivities that can be reached depending on the solid polymer configuration. The obtained results and the new insights provided by the model show the paths forward to improve the thermal insulation capabilities of nanocellular polymers.

Declaration of Competing Interest

The authors declare that they have no known competing financial interests or personal relationships that could have appeared to influence the work reported in this paper.

Acknowledgements

Financial assistance from the Junta of Castile and Leon grant (I. Sánchez-Calderón and VA202P20) is gratefully acknowledged. Financial support from the Spanish Ministry of Science, Innovation, and Universities (RTI2018-098749-B-I00 and PTQ2019-010560 (Victoria Bernardo-García)) is gratefully acknowledged. Financial support from the European Regional Development Fund of the European Union and of the Castile and Leon ((ICE): R&D PROJECTS IN SMEs: PAVIPEX. 04/18/VA/008 and M-ERA.NET PROJECT: FICACEL. 11/20/VA/0001) is gratefully acknowledged.

Appendix A. Supplementary data

Supplementary data to this article can be found online at https://doi.org/10.1016/j.matdes.2022.110938.

References

[1] International Energy Agency. Transition to Sustainable Buildings. Strategies and Opportunities to 2050, (2013).
[2] M. Casini, Smart Buildings. Advanced Materials and Nanotechnology to Improve Energy-Efficiency and Environmental Performance, 2016th ed., Woodhead Publishing, n.d.
[3] European Commission – Department: Energy – In focus. Energy efficiency in buildings, (2020).
[4] Directive 2010/31/EU of the European Parliament and of the Council of 19 May 2010 on the energy performance of buildings, (n.d.).
[5] Directive 2012/27/EU of the European Parliament and of the Council of 25 October 2012 on energy efficiency, amending Directives 2009/125/EC and 2010/30/EU and repealing Directives 2004/8/EC and 2006/32/EC, (n.d.).
[6] J. Wernery, F. Mancebo, W.J. Malfait, M. O'Connor, B.P. Jelle, The economics of thermal superinsulation in buildings, Energy Build. 253 (2021) 111506, https://doi.org/10.1016/j.enbuild.2021.111506.
[7] W. Villasmil, L.J. Fischer, J. Worlitschek, A review and evaluation of thermal insulation materials and methods for thermal energy storage systems, Renew. Sustain. Energy Rev. 103 (2019) 71–84, https://doi.org/10.1016/j.rser.2018.12.040.
[8] B. Notario, J. Pinto, E. Solorzano, J.A. de Saja, M. Dumon, M.A. Rodríguez-Pérez, Experimental validation of the Knudsen effect in nanocellular polymeric foams, Polymer (Guildf). 56 (2015) 57–67, https://doi.org/10.1016/j.polymer.2014.10.006.
[9] B. Notario, J. Pinto, M.A. Rodriguez-Perez, Nanoporous polymeric materials: A new class of materials with enhanced properties, Prog. Mater. Sci. 78–79 (2016) 93–139, https://doi.org/10.1016/j.pmatsci.2016.02.002.

[10] B. Xiang, Y. Jia, Y. Lei, F. Zhang, J. He, T. Liu, S. Luo, Mechanical properties of microcellular and nanocellular silicone rubber foams obtained by supercritical carbon dioxide, Polym. J. 51 (6) (2019) 559–568, https://doi.org/10.1038/s41428-019-0175-6.
[11] J. Martín-de León, V. Bernardo, M.Á. Rodríguez-Pérez, Key Production Parameters to Obtain Transparent Nanocellular PMMA, Macromol. Mater. Eng. 302 (12) (2017) 1700343, https://doi.org/10.1002/mame.201700343.
[12] G.Q. Lu, X.S. Zhao, Nanoporous Materials - An Overview, in: Nanoporous Mater. Sci, Eng., Imperial College Press, 2004, pp. 1–13, https://doi.org/10.1142/9781860946561_0001.
[13] S. Costeux, CO2-Blown nanocellular foams, J. Appl. Polym. Sci. 131 (23) (2014) n/a–n/a, https://doi.org/10.1002/app.41293.
[14] S. Liu, J. Duvigneau, G.J. Vancso, Nanocellular polymer foams as promising high performance thermal insulation materials, Eur. Polym. J. 65 (2015) 33–45, https://doi.org/10.1016/j.eurpolymj.2015.01.039.
[15] C. Forest, P. Chaumont, P. Cassagnau, B. Swoboda, P. Sonntag, Polymer nano-foams for insulating applications prepared from CO2 foaming, Prog. Polym. Sci. 41 (2015) 122–145, https://doi.org/10.1016/j.progpolymsci.2014.07.001.
[16] J. Martín-de León, V. Bernardo, M. Rodríguez-Pérez, Nanocellular Polymers: The Challenge of Creating Cells in the Nanoscale, Materials (Basel) 12 (2019) 797, https://doi.org/10.3390/ma12050797.
[17] J. Martín-de León, V. Bernardo, P. Cimavilla-Román, S. Pérez-Tamarit, M.Á. Rodríguez-Pérez, Overcoming the Challenge of Producing Large and Flat Nanocellular Polymers: A Study with PMMA, Adv. Eng. Mater. 21 (6) (2019) 1900148, https://doi.org/10.1002/adem.201900148.
[18] H. Yu, H. Zhang, J. Zhao, J. Liu, X. Xia, X. Wu, Thermal conductivity of micro/nano-porous polymers: Prediction models and applications, Front. Phys. 17 (2) (2022), https://doi.org/10.1007/s11467-021-1107-4.
[19] G. Wang, C. Wang, J. Zhao, G. Wang, C.B. Park, G. Zhao, Modelling of thermal transport through a nanocellular polymer foam: Toward the generation of a new superinsulating material, Nanoscale 9 (18) (2017) 5996–6009.
[20] V. Bernardo, J. Martin-de Leon, J. Pinto, U. Schade, M.A. Rodriguez-Perez, On the interaction of infrared radiation and nanocellular polymers: First experimental determination of the extinction coefficient, Colloids Surf. A Physicochem. Eng. Asp. 600 (2020) 124937, https://doi.org/10.1016/j.colsurfa.2020.124937.
[21] P. Buahom, C. Wang, M. Alshrah, G. Wang, P. Gong, M.-P. Tran, C.B. Park, Wrong expectation of superinsulation behavior from largely-expanded nanocellular foams, Nanoscale 12 (24) (2020) 13064–13085.
[22] L.J. Gibson, M.F. Ashby, Cellular Solids: Structure and Properties, Cambridge Univ. Press, Cambridge, 1997.
[23] M. Alvarez-Lainez, M.A. Rodriguez-Perez, J.A. DE Saja, Thermal Conductivity of Open-Cell Polyolefin Foams, J. Polym. Sci. Part B Polym. Phys. 46 (2) (2008) 212–221.
[24] L.W. Hrubesh, R.W. Pekala, Thermal properties of organic and inorganic aerogels, J. Mater. Res. 9 (3) (1994) 731–738, https://doi.org/10.1557/JMR.1994.0731.
[25] X. Lu, R. Caps, J. Fricke, C.T. Alviso, R.W. Pekala, Correlation between structure and thermal conductivity of organic aerogels, J. Non. Cryst. Solids. 188 (3) (1995) 226–234, https://doi.org/10.1016/0022-3093(95)00191-3.
[26] E. Solórzano, M.A. Rodriguez-Perez, J. Lázaro, J.A. de Saja, Influence of Solid Phase Conductivity and Cellular Structure on the Heat Transfer Mechanisms of Cellular Materials: Diverse Case Studies, Adv. Eng. Mater. 11 (10) (2009) 818–824, https://doi.org/10.1002/adem.200900138.
[27] O.A. Almanza, M.A. Rodríguez-Pérez, J.A. De Saja, Prediction of the radiation term in the thermal conductivity of crosslinked closed cell polyolefin foams, J. Polym. Sci. Part B Polym. Phys. 38 (2000) 993–1004, https://doi.org/10.1002/(SICI)1099-0488(20000401)38:7<993::AID-POLB10>3.0.CO;2-J.
[28] N.C. Hilyard, A. Cunningham, Low density cellular plastics Physical basis of behaviour, 1994. https://doi.org/10.1007/978-94-011-1256-7.
[29] V. Bernardo, J. Martin-de Leon, J. Pinto, R. Verdejo, M.A. Rodriguez-Perez, Modeling the heat transfer by conduction of nanocellular polymers with bimodal cellular structures, Polymer (Guildf). 160 (2019) 126–137, https://doi.org/10.1016/j.polymer.2018.11.047.
[30] P. Scheuerpflug, M. Hauck, J. Fricke, Thermal properties of silica aerogels between 1.4 and 330 K, J. Non. Cryst. Solids. 145 (1992) 196–201, https://doi.org/10.1016/S0022-3093(05)80455-7.
[31] H. Ebert, Thermal Properties of Aerogels, in, Aerogels Handb. (2011) 537–564, https://doi.org/10.1007/978-1-4419-7589-8.
[32] J. Fricke, E. Hümmer, H.-J. Morper, P. Scheuerpflug, Thermal Properties Of Silica Aerogels, Le, J. Phys. Colloq. 24 (C4) (1989) C4-87–C4-97, https://doi.org/10.1051/jphyscol:1989414.
[33] J. Fricke, Aerogels, in: Springer Proc. Phys. 6, 1985.
[34] J. Fricke, Thermal Transport in Porous Superinsulations, (1986) 94–103. https://doi.org/10.1007/978-3-642-93313-4_11.
[35] Z.-Y. Li, C.-Y. Zhu, X.-P. Zhao, A theoretical and numerical study on the gas-contributed thermal conductivity in aerogel, Int. J. Heat Mass Transf. 108 (2017) 1982–1990, https://doi.org/10.1016/j.ijheatmasstransfer.2017.01.051.
[36] S. Song, M.M. Yovanovich, F.O. Goodman, Thermal gap conductance of conforming surfaces in contact, J. Heat Transfer. 115 (1993) 533–540, https://doi.org/10.1115/1.2910719.
[37] Y.L. He, T. Xie, Advances of thermal conductivity models of nanoscale silica aerogel insulation material, Appl. Therm. Eng. 81 (2015) 28–50, https://doi.org/10.1016/j.applthermaleng.2015.02.013.
[38] S. Sonnick, L. Erlbeck, M. Meier, H. Nirschl, M. Rädle, Methodical selection of thermal conductivity models for porous silica-based media with variation of gas type and pressure, Int. J. Heat Mass Transf. 187 (2022) 122519, https://doi.org/10.1016/j.ijheatmasstransfer.2022.122519.
[39] J. Nassios, Kinetic theory of rarefied gas flows with modern applications, Austms.Org.Au. (2006). https://www.austms.org.au/Publ/Gazette/2013/Mar13/Nassios.pdf.
[40] S.E. Kentish, C.A. Scholes, G.W. Stevens, Carbon Dioxide Separation through Polymeric Membrane Systems for Flue Gas Applications, Recent Patents, Chem. Eng. 1 (1) (2010) 52–66, https://doi.org/10.2174/1874478810801010052.
[41] R. Siegel, J.R. Howell, Thermal Radiation Heat Transfer, Taylor & Francis, London, 1992.
[42] R.A. Campo-Arnáiz, M.A. Rodríguez-Pérez, B. Calvo, J.A. de Saja, Extinction coefficient of polyolefin foams, J. Polym. Sci. Part B Polym. Phys. 43 (13) (2005) 1608–1617, https://doi.org/10.1002/polb.20435.
[43] L. Glicksman, M. Schuetz, M. Sinofsky, Radiation heat transfer in foam insulation, Int. J. Heat Mass Transf. 30 (1) (1987) 187–197, https://doi.org/10.1016/0017-9310(87)90071-8.
[44] J. Martín-de León, J.L. Pura, V. Bernardo, M.Á. Rodríguez-Pérez, Transparent nanocellular PMMA: Characterization and modeling of the optical properties, Polymer (Guildf). 170 (2019) 16–23, https://doi.org/10.1016/j.polymer.2019.03.010.
[45] A.J. Cox, A.J. DeWeerd, J. Linden, An experiment to measure Mie and Rayleigh total scattering cross sections, Am. J. Phys. 70 (6) (2002) 620–625, https://doi.org/10.1119/1.1466815.
[46] J. Wang, D. Petit, S. Ren, Transparent thermal insulation silica aerogels, Nanoscale Adv. 2 (12) (2020) 5504–5515.
[47] B. Merillas, J. Martín-de León, F. Villafañe, M.A. Rodríguez-Pérez, Transparent Polyisocyanurate-Polyurethane-Based Aerogels: Key Aspects on the Synthesis and Their Porous Structures, ACS Appl. Polym. Mater. 3 (9) (2021) 4607–4615, https://doi.org/10.1021/acsapm.1c00712.
[48] U. Heinemann, R. Caps, J. Fricke, Radiation-conduction interaction : An investigation on silica aerogels, Int. J. Heat Mass Transf. 39 (1996) 2115–2130, https://doi.org/10.1016/0017-9310(95)00313-4.
[49] F. Almeida, H. Beyrichen, N. Dodamani, R. Caps, A. Muller, R. Oberhoffer, Thermal conductivity analysis of a new sub-micron sized polystyrene foam, (2020). https://doi.org/10.1177/0021955X20943101.
[50] Y. Jannot, A. Degiovanni, V. Grigorova-Moutiers, J. Godefroy, A passive guard for low thermal conductivity measurement of small samples by the hot plate method, Meas. Sci. Technol. 28 (1) (2017) 015008, https://doi.org/10.1088/1361-6501/28/1/015008.
[51] V. Bernardo, J. Martín-de León, M.Á. Rodríguez-Pérez, Production of PMMA-based nanocellular polymers using low demanding saturation conditions, Mater. Lett. 255 (2019) 126551, https://doi.org/10.1016/j.matlet.2019.126551.
[52] I. Sánchez-Calderón, V. Bernardo, M. Santiago-Calvo, H. Naji, A. Saiani, M. Rodríguez-Pérez, Effect of the molecular structure of TPU on the cellular structure of nanocellular polymers based on PMMA/TPU blends, Polymers (Basel). 13 (18) (2021) 3055, https://doi.org/10.3390/polym13183055.
[53] V. Kumar, N.P. Suh, A process for making microcellular thermoplastic parts, Polym. Eng. Sci. 30 (20) (1990) 1323–1329, https://doi.org/10.1002/pen.760302010.
[54] J. Pinto, E. Solórzano, M.A. Rodriguez-Perez, J.A. de Saja, Characterization of the cellular structure based on user-interactive image analysis procedures, J. Cell. Plast. 49 (6) (2013) 555–575, https://doi.org/10.1177/0021955X13503847.
[55] V. Kumar, Process synthesis for manufacturing microcellular thermoplastic parts, Massachusetts Inst. Technol. (1988).
[56] ASTM C518 Standard Test Method for Steady-State Thermal Transmission Properties by Means of the Heat Flow Meter Apparatus, (2017).
[57] ISO 8301 Thermal insulation - Determination of steady-state thermal resistance and related properties - Heat flow meter, (1991).
[58] Y.A. Cengel, A.J. Ghajar, Heat and Mass Transfer: Fundamentals & Applications, Fifth Edit, Mc Graw Hill Education, 2006.
[59] J.R.G. Evans, P.G. Collishaw, Review: An assessment of expressions for the apparent thermal conductivity of cellular materials, J. Mater. Sci. 29 (1994) 2261–2273.
[60] J.A. Reglero Ruiz, C. Saiz-Arroyo, M. Dumon, M.A. Rodríguez-Perez, L. Gonzalez, Production, cellular structure and thermal conductivity of microcellular (methyl methacrylate)-(butyl acrylate)-(methyl methacrylate) triblock copolymers, Polym. Int. 60 (1) (2011) 146–152, https://doi.org/10.1002/pi.2931.